

EXPERIMENTAL STUDY OF RESONANCE CROSSING WITH A PAUL TRAP

H. Sugimoto, KEK, Ibaraki, Japan

Abstract

The resonant instability of charged particle beams during betatron resonance crossing is systematically investigated by both an experimental and a numerical approach. The present experiment is based on the fact that charged particle beams observed from its rest frame are almost equivalent to single-species plasmas confined in a plasma trap system. Tune excursion in a Non-Scaling Fixed-Field Alternating Gradient (NS-FFAG) accelerator with many identical FODO cells is emulated by ramping the plasma confinement force. It is experimentally and numerically confirmed that the resonance crossing is not harmful as long as the crossing speed is sufficiently high. We also address that a linear coherent stop band around quarter-half integers severely limits the machine performance at high-density beams. This band exists even without machine imperfection, thus the performance of NS-FFAGs is restricted as in high-power synchrotron accelerators.

INTRODUCTION

NS-FFAG [1] accelerators are expected to be a candidate for use in muon acceleration, as well as for medical purposes based on carbon and proton hadron therapy owing to their possibility of high repetition rate. One of the fundamental subjects in NS-FFAG is resonance crossing. The beam orbit and optics in NS-FFAG is widely varied during acceleration because guiding and focusing forces felt by the beam depend on the beam energy. Consequently, the beam transverses a few or more resonances before extraction and the resonance crossing may lead to serious beam losses or degradation of beam quality. Past theoretical and numerical studies suggest that emittance growth is negligible or tolerable when the crossing speed is sufficiently high [2].

In this study, we carry out systematic experiments on betatron resonance crossing without using any accelerators, but using a novel experimental tool named “S-POD (Simulator for Particle Orbit Dynamics)” developed at the Beam Physics Laboratory at Hiroshima University. S-POD is based on the physical equivalence between non-neutral plasmas in a plasma trap and charged particle beams propagating a linear focusing channel [3]. Particle-in-Cell (PIC) simulation corresponding to this experiment is also conducted. Based on a large number of experimental and numerical observations, we discuss the fundamental feature of resonance crossing including space-charge-driven resonances.

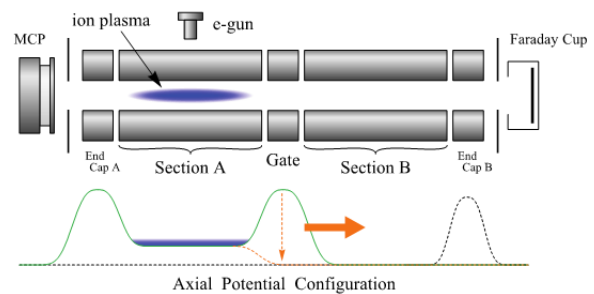
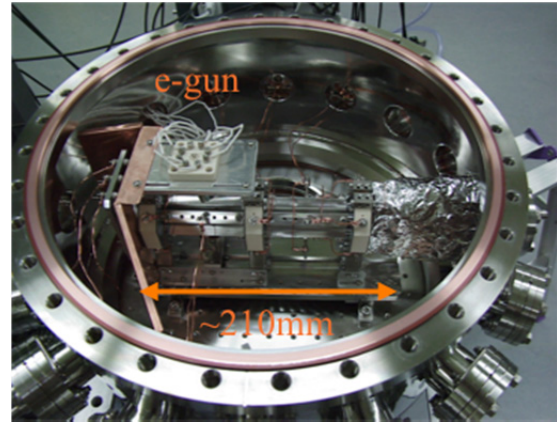


Figure 1: The linear Paul trap developed at the Hiroshima University and its schematic.

S-POD

Principle

Figure 1 shows the S-POD apparatus employed for the present experiment. S-POD is basically a linear Paul trap (LPT) system, and composed of five quadrupole-electrode sections. For the present experiment, ions are confined within the Section A as indicated in the lower panel of Fig.1. Similar to conventional LPTs, the plasma confinement in transverse (x - and y -) direction is achieved by an applied radio-frequency (rf) electric field with quadrupole symmetry. Static voltages are also applied to these electrodes to form a potential barrier for the longitudinal plasma confinement. Since the aperture size (5mm in radius) is much shorter than the longitudinal dimension of the confinement region (75mm), the potential barrier is square-well-like rather than harmonic. It is thus reasonably expected that the plasma is an infinitely long charge column along the longitudinal direction. This fact enables us to focus on betatron beam dynamics in the present study.

As stated above, transverse two-dimensional (2D) model is valid in analysis of the present experimental data. In the 2D model, the transverse motion of individual particles of the rest mass M and charge q is governed by the Hamiltonian

$$H = \frac{p_x^2 + p_y^2}{2} + \frac{1}{2}K_x(\tau)x^2 + \frac{1}{2}K_y(\tau)y^2 + \frac{q}{Mc}\phi^{sc}(x,y;\tau), \quad (1)$$

where c is the speed of light in vacuum, $K_{x,y}(\tau)$ is a "lattice function" which is proportional to the rf voltage on the quadrupole electrodes, and the independent variable is $\tau = ct$. The scalar potential ϕ^{sc} is associated to self-space-charge field satisfies the Vlasov-Poisson Equations. The Hamiltonian Eq. (1) is mathematically identical to that employed to theoretical study of space-charge effects in a longitudinally unbunched beam, hence we can use a plasma trap as an experimental tool for study the fundamental physics of charged particle beams.

Experiment Setup

Since the sinusoidal focusing system and FODO lattice have almost identical stop-band structures, the sinusoidal waveform is applied to $K_{x,y}(\tau)$ in the present study, and its frequency is chosen to be 1MHz. We assume a symmetric focusing lattice, namely $K_y(\tau) = -K_x(\tau) = -K(\tau)$ for simplicity. An application of S-POD to asymmetric doublet can be found in, for example, Ref. [4]. A circular accelerator composed of 42 doublet cells just like the NS-FFAG "EMMA" [5] is assumed. In this case, 42 sinusoidal rf periods correspond to one turn of the ring. Tune variation can be easily emulated by linearly ramping the rf voltage of the sinusoidal wave. The nominal tune excursion range is from $\nu_0 = 0.40$ to 0.17 per one cell. The corresponding rf voltages for the S-POD experiment are 88 V and 54 V, respectively. For instance, if the acceleration time in EMMA is assumed to be 10 turns, we take $1\mu\text{sec} \times 42 \times 10 = 0.42$ msec to ramp the rf amplitude.

In the experiment, $^{40}\text{Ar}^+$ ions are generated by electron impact ionization with an electron gun that ionizes neutral ^{40}Ar gas in the trap region. The initial plasma density can be controlled by adjusting the electron current or the Ar gas pressure. After the voltage ramping, the plasma is dumped to the Faraday cup (FC) by switching the DC bias on the one side of quadrupole electrodes.

Although in this paper we assume that EMMA has perfect lattice symmetry, it is possible to investigate the effect of lattice asymmetry by superimposing one or more perturbation waves with lower frequency [6,7]. In addition to gradient error of quadrupole magnets, we can examine the effects of dipole error field by exciting the quadrupole-electrodes with dipole configuration [8].

MULTI-PARTICLE SIMULATIONS

To support and guide experiment, we have performed systematic multi-particle simulations using the PIC code WARP [9]. Since our trap system well reproduces longitudinally unbunched beam as stated, we conducted 2D transverse beam dynamic simulation to save

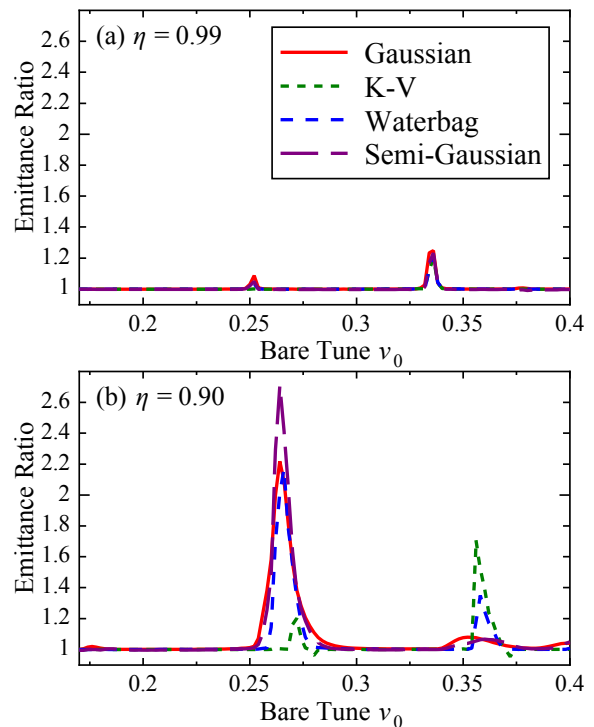


Figure 2: Stop-band distribution in S-POD obtained from WARP simulation for four different classes of initial distributions. The initial tune depressions η are chosen to be (a) 0.99 and (b) 0.90.

computational resources. The WARP field-solver calculates both external- and self-fields by solving the Poisson equation with conducting electrode boundaries. In the S-POD experiments, the electron gun is turned on for a few seconds to generate $^{40}\text{Ar}^+$ ions. It is practically impossible to perform a simulation of such long-time scale evolution. Therefore we here launch a beam matched to the focusing system and see how does it evolves.

Provided that the system has no mechanical alignment errors, every fourth multipole harmonic rf components (quadrupole, dodecapole, ...) are present. However, the actual trap inevitably contains alignment errors that likely amplify nonlinear fields. To take into account this effect, we artificially introduce first two nonlinear fields (sextupole and octupole) in the following simulations without particularly noted. Their amplitudes relative to the quadrupole field at the aperture radius 5 mm are 0.66 % and 0.42 %, respectively.

Stop-band Distribution

The stop-band distributions in S-POD four different initial distributions, K-V, Gaussian, Waterbag and Semi-Gaussian are shown in Figure 2. The initial tune depressions η are 0.99 and 0.90 for Fig. 2 (a) and (b), respectively. The ordinates represent the ratio of the rms emittance after 100 rf periods (0.1 msec). There are two notable resonances at $\nu_0 \sim 1/3$ and $1/4$. According to a linearized Vlasov theory for 1D sheet-beams, coherent resonant instabilities are excited under the condition [10]

$$(\nu_0 - C_m \Delta\nu) \approx \frac{n}{2m}, \quad (4)$$

where m and n are both integers, ν_0 and $\Delta\nu$ are the bare betatron tune and the incoherent tune shift due to space charge. C_m is a constant smaller than unity which depends on the mode number m . At low density, the instability at $\nu_0 \sim 1/4$ is mainly due to a fourth-order resonance associated to electrode misalignment, while at high density the instability is mainly caused by a second order ($m=2$) resonance, which is well-known as “envelope instability”. The emittance growth at $\nu_0 \sim 1/3$ is caused by third-order resonances ($m=3$) enhanced by the mechanical misalignment of the electrodes. This instability is attributed to sixth-order resonance also because the cylindrical electrodes inevitably generate the six-order driving force as well. In the low-density case, the resonance at $\nu_0 \sim 1/3$ shows the largest emittance growth. While in the high-density case, the emittance growth caused by resonance at $\nu_0 \sim 1/4$ exceeds that caused by the third-order resonance.

Resonance Crossing

Figure 3 shows typical simulation results of resonance crossing in the corresponding doublet cell, where emittance evolution during the tune excursion at two different initial tune depressions η is plotted. Four different classes of initial distributions are studied. In the case of Fig. 3(a), the amount of emittance growth caused by crossing two resonances at $\nu_0 \sim 1/3$ and $\nu_0 \sim 1/4$ are comparable. While in the high-density case of Fig. 3(b), the quarter-half-integer resonance plays a major role. The K-V beam is the most stable simply because it has the weakest quarter-half-integer resonance among the all four distributions as shown in Fig. 2. It is shown later in Fig. 4 that it becomes unstable rapidly when the crossing speed or the tune depression exceeds threshold values. The Gaussian beam, which is likely the most realistic distribution shows the largest emittance growth owing to its wide and strong resonance band as shown in Fig. 2.

Quarter-half-integer Resonance Crossing

Since the crossing of the linear coherent instability at the quarter-half-integer causes serious beam degradation at high-density beams. It is informative to show how the emittance growth depends on the fundamental parameters of the resonance crossing including the class of beam distribution. We here numerically investigate the emittance growth caused by the quarter-half-integer resonance crossing. The tune sweeping range is chosen to be from $\nu_0 = 0.31$ to 0.23 so that the beam crosses only this resonance. The nonlinear fields associated with the electrodes misalignment are not included in the simulations.

Figure 4 summarizes the results of the numerical campaign, where emittance growth as a function of the initial tune depression for several crossing speeds and initial distribution types are plotted. We here defined the dimensionless crossing speed parameter $u \equiv \delta/n_{\text{rf}}$, where

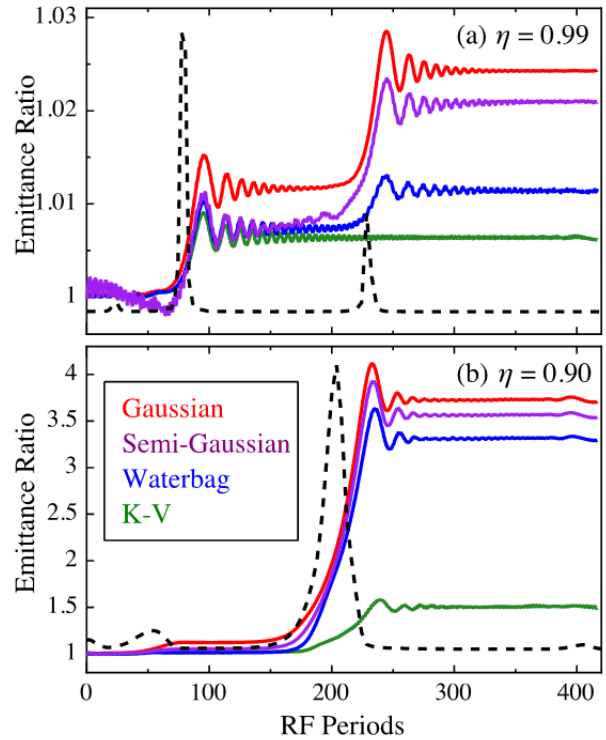


Figure 3: Emittance evolution during resonance crossing for four different classes of initial distributions at two different initial tune depressions. For reference, the corresponding stop-band distributions of the Gaussian beam are added to each panel with broken lines.

δ is the tune variation width and n_{rf} is the number of rf focusing period for the tune excursion. The open circle shown in Fig. 4(a) is the results obtained with the FODO lattice instead of the sinusoidal focusing system. The FODO lattice and sinusoidal focusing lattice gives almost same amount of emittance growth as expected, simply because their resonance structures are identical as mentioned. All distribution types show qualitatively same tendency, namely the slower crossing or/and higher particle density causes larger emittance increment. We see that the emittance growth for all distributions except for K-V almost linearly depends on tune depression as long as the effect from particle losses is negligible. The K-V beam becomes unstable rapidly when these parameters exceed threshold values.

EXPERIMENTS

Stop-band Distribution

Before proceeding to resonance crossing experiments, we examine the stop-band distribution of S-POD analogous to Fig. 2. The results are obtained by carrying out tune survey on number of $^{40}\text{Ar}^+$ ions surviving after 10 msec storage. Experimental results at three different

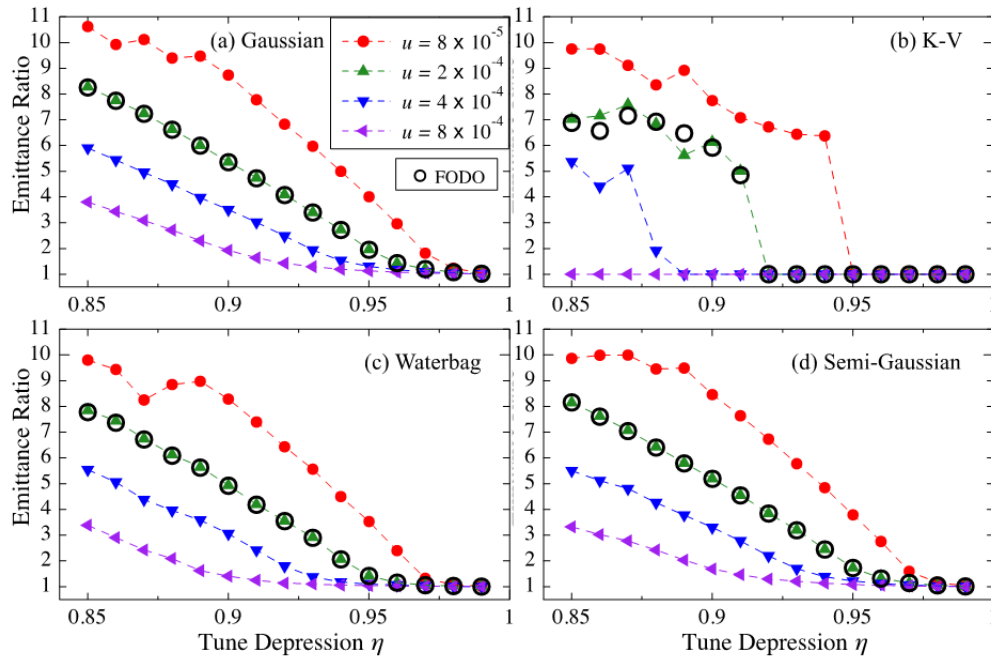


Figure 4: Emittance growth caused by crossing of the quarter-half-integer resonance.

initial ion number N_{in} are summarized in Fig. 5. A separate PIC simulation shows that the experimental band locations are consistent with the PIC simulations [7]. We can roughly estimate the tune depression of the plasma by comparing the band location of the experimental and simulation data. For instance, the tune depression is likely about $0.85 \sim 0.9$ when $N_{in} \sim 10^7$.

Resonance Crossing

Figure 6 shows survived ion number after resonance crossing at various crossing speeds. The vertical broken line in Fig. 6 indicates $u = 5.48 \times 10^{-4}$ corresponds to 10 turns extraction from the EMMA ring. In the highest-density case (red dots), a significant number of ions are lost even with rather fast crossing speed while there is no serious ion loss in other two cases when the crossing

speed is sufficiently high. For instance, only the highest-density case shows noticeable ions loss at 10 turns beam extraction.

A fundamental question raised from Fig. 6 is which stop band is the most responsible for the observed ion loss. Single resonance crossing experiment is carried out to answer this question. Figure 7 summarizes experimental results at three different tune sweeping ranges, where initial and final tunes are chosen to be (a) (0.4, 0.32), (b) (0.31, 0.23) and (c) (0.22, 0.14). These ranges are selected so that the beam transverse a particular stop band observed in Fig. 5. The experiments are carried out with three different initial ion numbers of $N_{in} \sim 10^5$, 10^6 and 10^7 . In the lowest-density case, the noticeable ion loss is observed only at case (a), which implies the ion loss shown in Fig. 6 is likely due to third-order resonance enhanced by the mechanical misalignment of the electrodes. Strictly speaking, this instability may be attributed to sixth-order resonance also. It is difficult to assert which one is stronger or weaker because the exact configuration of the electrodes is not known. In the highest-density case, the effect from the linear coherent resonance is increased noticeably as shown in case (b). This resonance is strong in general, and inevitably exists even when the machine has no machine imperfection. Therefore, this resonant instability may limit the quality of all high-density NS-FFAG beams.

SUMMARY

A systematic study on betatron resonance crossing has been conducted with the novel experimental tool S-POD developed at Hiroshima University. The S-POD system approximately emulates charged particle beams

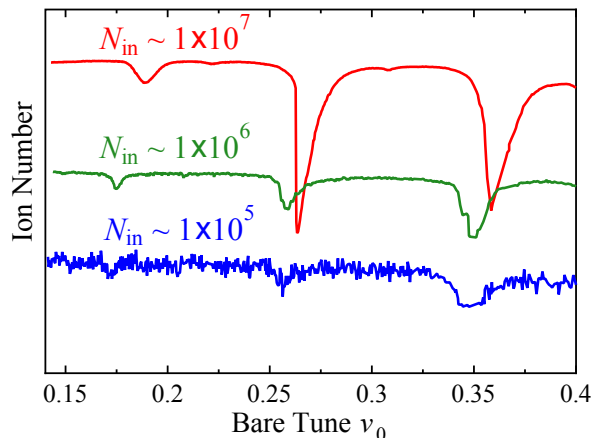


Figure 5: Stop-band distributions obtained from a large number of S-POD experiments.

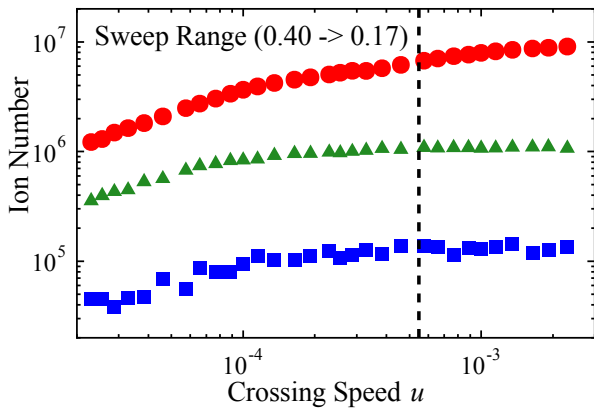


Figure 6: Survived ion number after resonance crossing as a function of crossing speed.

propagating linear beam transport channels and enables us to study a wide variety of fundamental beam physics without a large scale and expensive hardware. By utilizing the advantages, resonance crossing in NS-FFAG is simulated with a wide range of beam densities, sweeping speeds and widths. We also carried out a large number of PIC simulations to support and interpret the experimental observations.

The stop-band distribution of the FODO cell emulated by the sinusoidal wave is obtained with both experiments and numerical simulations. The results show that there are three noticeable stop bands at $\nu_0 \sim 1/3$, $1/4$ and $1/6$. Third- and sixth-order resonances are likely responsible for the bands at $\nu_0 \sim 1/3$ and $1/6$. At low density, the instability at $\nu_0 \sim 1/4$ is mainly due to a fourth-order resonance associated to electrode misalignment, while at high density the instability is attributed to a second-order coherent resonance driven by space charge.

Systematic numerical study on the emittance growth caused by crossing of the quarter-half-integer resonance was conducted. It has confirmed that slower crossing or higher particle density results larger emittance growth regardless to the initial distribution type. We also showed that the FODO lattice and the sinusoidal focusing system results almost identical emittance growth.

As predicted by past theoretical and numerical studies, the resonance crossing is not harmful as long as the beam is extracted before the resonant instability grows. The required crossing speed naturally depends on the strength of the resonance. At the high-density beams, the second-order resonance at $\nu_0 \sim 1/4$ has serious effects and, it inevitably exists even without machine imperfection, thus it may limit the performance of next-generation high-power NS-FFAGs.

ACKNOWLEDGMENTS

The present S-POD experiment was carried out by the Beam Physics Laboratory at Hiroshima University. The author is indebted to K. Ito and H. Okamoto for providing the experimental data and valuable comments. The author would also like to thank K. Fukushima for his assistance on WARP simulation. The S-POD project was supported

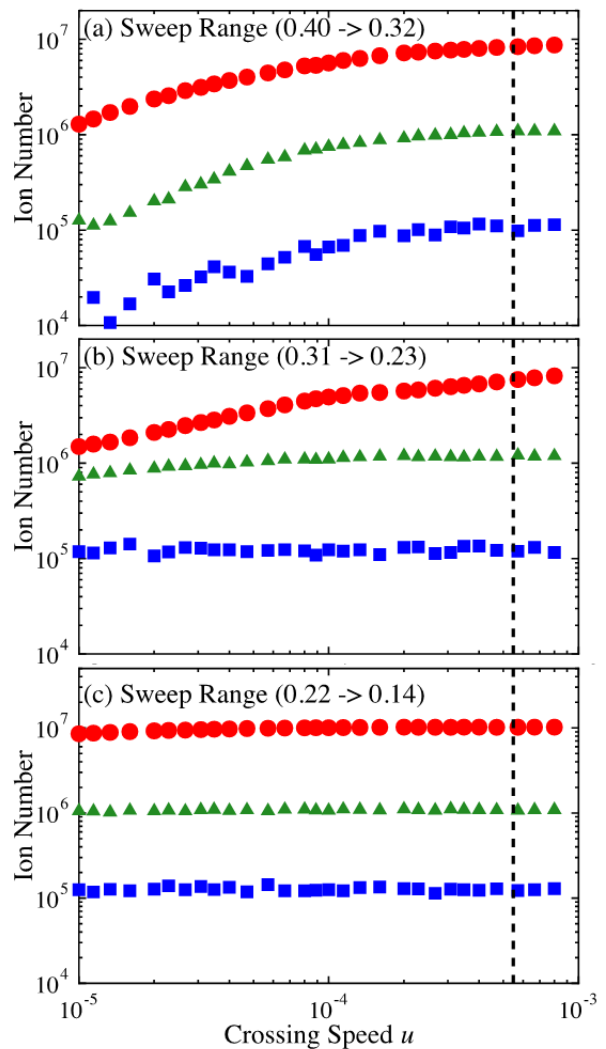


Figure 7: Survived ion number after a particular resonance crossing as a function of crossing speed.

in part by a Grant-in-Aid for Scientific Research, Japan Society for the Promotion of Science.

REFERENCES

- [1] C. Johnstone, W. Wan, A. Garren, PAC'99, 3068.
- [2] S. Machida, Phys. Rev. STAB 11, 094003 (2008).
- [3] H. Okamoto and H. Tanaka, Nucl. Instrum. Meth. A 437 (1999) 178.
- [4] K. Fukushima et al., Nucl. Instrum. Meth. A, to be published.
- [5] S. Machida et al., Nature Physics 8, 243-247, (2012).
- [6] S. Ohtsubo, et al., Phys. Rev. STAB 13, 044201 (2010).
- [7] H. Takeuchi, et al., Phys. Rev. STAB 15, 074201 (2012).
- [8] S.L. Sheehy et al., IPAC'13 2677.
- [9] P. Grote, Ph.D. thesis, University of California at Davis, 1994.
- [10] H. Okamoto and K. Yokoya, Nucl. Instrum. Meth. A 482 (2002) 51.